

Soft Contact Manipulation of a Rigid Object Using Multibond Graph

Rahul RATHEE¹⁾, Anil Kumar NARWAL^{1)*}, Anand VAZ²⁾

¹⁾ *Department of Mechanical Engineering
Deenbandhu Chhotu Ram University of Science and Technology
Murthal, Sonapat 131039, Haryana, India; e-mail: rahulrathee4@gmail.com
Corresponding Author e-mail: aknarwal@dcrustm.org

²⁾ *Department of Mechanical Engineering
Dr. B. R. Ambedkar National Institute of Technology
Jalandhar 144011, Punjab, India; e-mail: anandvaz@ieee.org*

Dexterous manipulation of a rigid object using artificial soft fingers is not easy to achieve. Instantaneous contact areas and the distribution of contact forces at the interfaces change dynamically during the soft contact manipulation of the object. A bond graph model for dynamics of the soft contact manipulation of a rigid object using two soft pads is developed. A cylindrical disc is used as the rigid object to be manipulated between two soft silicon rubber pads considered in place of soft fingertips, one above and the other below. The disc is grasped and rolled between the two pads so its center follows a desired horizontal displacement trajectory. A closed-loop feedback control system generates the required force to grasp and control the instantaneous position of the disc's center. The model determines the instantaneous contact forces required for the desired manipulation. Simulation results validate the model.

Keywords: soft contact manipulation, multibond graph, FEM, soft fingertips, rigid body dynamics.

NOTATION

- CM – center of mass,
- ${}^0\overline{W}_D$ – weight of the disc,
- L_x – length of the soft pads,
- L_y – height of the soft pads,
- C_{Br} – center of mass of the bracket,
- N – total number of nodes in each soft pad,
- NT_L – the number of non-contacting nodes of the lower soft pad,
- NT_U – the number of non-contacting nodes of the upper soft pad,
- B – the number of fixed nodes at the bottom layer of the lower pad,

- M_L – the number of movable nodes in the lower pad,
 M_U – the number of movable nodes in the upper pad,
 N_{Br} – the number of nodes of the upper pad which are rigidly attached to the bracket,
 T_L, T_U – total number of instantaneous contacting nodes of the lower and the upper pad, respectively,
 \bar{e}_n – effort vector corresponding to n -th multibond,
 \bar{f}_n – flow vector corresponding to n -th multibond,
 L_i – any i -th node on the top layer of the lower pad,
 U_j – any j -th node on the bottom layer of the upper pad,
 S_i – re-designation of the node L_i on the top layer of the lower soft pad once it comes in contact with the disc,
 V_j – re-designation of node U_j on the bottom layer of the upper soft pad once it comes in contact with the disc,
 P_i – point of contact of S_i -th node at the disc periphery,
 Q_j – point of contact of V_j -th node at the disc periphery,
 ${}^A_B\bar{r}_C$ – the position of point C with respect to point B expressed in the frame $\{\mathbf{A}\}$; $\in \mathbb{R}^{3 \times 1}$,
 ${}^0_{S_i}\bar{r}_{P_i}$ – the position of the point P_i with respect to the node S_i expressed in the inertial frame $\{\mathbf{O}\}$; $\in \mathbb{R}^{3 \times 1}$,
 ${}^0_{V_j}\bar{r}_{Q_j}$ – the position of the point Q_j with respect to the node V_j expressed in the inertial frame $\{\mathbf{O}\}$; $\in \mathbb{R}^{3 \times 1}$,
 ${}^0\bar{r}_C$ – the position of the CM of the disc observed and expressed in the inertial frame $\{\mathbf{O}\}$; $\in \mathbb{R}^{3 \times 1}$,
 ${}^0\bar{r}_{L_i}$ – the position of the node L_i observed and expressed in the inertial frame $\{\mathbf{O}\}$; $\in \mathbb{R}^{3 \times 1}$,
 ${}^0\bar{r}_{U_j}$ – the position of the node U_j observed and expressed in the inertial frame $\{\mathbf{O}\}$; $\in \mathbb{R}^{3 \times 1}$,
 ${}^0_i R$ – the rotational matrix that determines the orientation of the i -th moving frame with respect to the inertial frame $\{\mathbf{O}\}$; $\in \mathbb{R}^{3 \times 3}$,
 ${}^0\bar{\omega}_D$ – the angular velocity of the disc observed and expressed in the inertial frame $\{\mathbf{O}\}$; $\in \mathbb{R}^{3 \times 1}$,
 ${}^i_{S_i}\dot{\bar{r}}_{P_i}$ – the relative velocity of the point P_i with respect to the node S_i , observed and expressed in the i -th moving frame; $\in \mathbb{R}^{3 \times 1}$,
 ${}^j_{V_j}\dot{\bar{r}}_{Q_j}$ – the relative velocity of the point Q_j with respect to the node V_j , observed and expressed in the j -th moving frame; $\in \mathbb{R}^{3 \times 1}$,
 ${}^0_{S_i}\dot{\bar{r}}_{P_i}$ – the relative velocity of the point P_i with respect to the node S_i , observed and expressed in the inertial frame $\{\mathbf{O}\}$; $\in \mathbb{R}^{3 \times 1}$,
 ${}^0_{V_j}\dot{\bar{r}}_{Q_j}$ – the relative velocity of the point Q_j with respect to the node V_j , observed and expressed in the inertial frame $\{\mathbf{O}\}$; $\in \mathbb{R}^{3 \times 1}$,
 ${}^0\dot{\bar{r}}_C$ – the velocity of the CM of the disc observed and expressed in the inertial frame $\{\mathbf{O}\}$; $\in \mathbb{R}^{3 \times 1}$,
 ${}^0\bar{F}_{P_i}$ – contact forces on the point P_i , expressed in inertial frame $\{\mathbf{O}\}$; $\in \mathbb{R}^{3 \times 1}$,
 ${}^0\bar{F}_{Q_j}$ – contact forces on the point Q_j , expressed in inertial frame $\{\mathbf{O}\}$; $\in \mathbb{R}^{3 \times 1}$,
 ${}^0\bar{F}_D$ – total contact force that acts on the disc, expressed in inertial frame $\{\mathbf{O}\}$; $\in \mathbb{R}^{3 \times 1}$,
 ${}^0\bar{p}_D$ – translational momentum of the disc, expressed in inertial frame $\{\mathbf{O}\}$; $\in \mathbb{R}^{3 \times 1}$,
 ${}^0_C\bar{p}_D$ – the angular momentum of the disc, about its CM, expressed in inertial frame $\{\mathbf{O}\}$; $\in \mathbb{R}^{3 \times 1}$,
 ${}^0_C I_D$ – inertia tensor of the disc about its CM, expressed in the inertial frame $\{\mathbf{O}\}$; $\in \mathbb{R}^{3 \times 3}$,
 $[I_L]$ – inertia matrix of the lower pad; $[I_L] \in \mathbb{R}^{2(N-B) \times 2(N-B)}$,
 $[I_U]$ – inertia matrix of the upper pad; $[I_U] \in \mathbb{R}^{2(N-N_{Br}) \times 2(N-N_{Br})}$,

$C : [K_L]^{-1}$ – stiffness matrix of the lower pad; $[K_L] \in \mathbb{R}^{2N \times 2N}$,
 $C : [K_U]^{-1}$ – stiffness matrix of the upper pad; $[K_U] \in \mathbb{R}^{2N \times 2N}$,
 $R : [R_L]$ – damping matrix for the lower pad; $[R_L] \in \mathbb{R}^{2N \times 2N}$,
 $R : [R_U]$ – damping matrix for the upper pad; $[R_U] \in \mathbb{R}^{2N \times 2N}$,
 $\overline{M}_{C_{Br}}$ – moment that acts on the bracket about its CM.

1. INTRODUCTION

The human hand has the capabilities to handle and manipulate various objects with dexterity. Object manipulation involves grasping, sliding, and rolling the object using soft fingers. A rigid object develops area contacts at the interfaces while manipulating it with the soft pulped fingers of the human hand. The contact areas and distribution of contact forces over them vary with time as the contact interfaces change during object manipulation. Soft pulp deforms dynamically and tends to conform to the geometry of the rigid object during manipulation [1]. The mechanics of object manipulation using soft fingers involves determining the contact areas and distribution of contact forces over them, the deformation of the soft pulp, and moments of the contact forces on the manipulated object [2]. The determination of forces and moments to be applied at the contact interfaces on the rigid object is required to achieve its accurate manipulation. Therefore, the soft contact manipulation of a rigid object is quite challenging.

Contact between two rigid bodies is generally considered a point contact, although it is always an area contact in actual physical systems, due to the non-existence of a perfectly rigid body. The assumption of point contact simplifies calculations but only provides approximate solutions to contact problems [3]. The concept of a point contact was used to solve the mechanics of object manipulation in [4]. The Hertz contact model provides the foundation for developing different contact theories that involve area contact. The model was developed for an area contact between an elastic sphere and a plane rigid surface [5]. Johnson *et al.* [6] included interfacial adhesion in the model and concluded that interfacial surface energy plays an important role in intermittent area contacts. Most of the existing contact models consider static contact between two bodies. Static contact implies that the rigid body is in resting contact with the soft material, and the contact interface does not change with time. However, contact interfaces change dynamically while handling or manipulating objects using soft fingers. Hence, it is important to model the dynamics of continuously changing contacts between the object and soft fingers.

The authors have previously modeled the contact dynamics between a rigid body and a soft material pad using the bond graph approach [7]. The bond graph is a graphical representation of the physical system dynamics. It is developed

based on the flow of power and information between component subsystems of a physical system and represents causality elegantly. The nuances of bond graph modeling of the dynamics of physical systems are available in several references [8–10]. A rigid body has six degrees of freedom in space, while a soft material pad, being in the continuum, has infinite degrees of freedom [11]. The continuum properties of the soft material were discretized using the finite element method (FEM). The accuracy of the results increases with the number of degrees of freedom. The soft material pad's stiffness and mass matrices were calculated and used as \mathbf{C} and \mathbf{I} fields in the bond graph model [11]. The developed model is valid for any geometry of the rigid body and the material of the soft pad. It was also validated experimentally for static contact [7, 12]. The model was simulated for circular and non-circular geometries of rigid bodies. The dynamics of the soft contact interaction for a circular disc rolling over the soft material pad were evaluated. The model determines the contact area and distribution of the contact forces over it, which change dynamically as the disc rolls over the soft pad. Dynamics of soft contact interaction of an elliptical disc and a cuboidal block that fall freely from an inclined resting position on the soft pad was also simulated using the developed model [7, 13, 14]. Dynamics of impact contact when a spherical ball falls freely on a soft silicon rubber pad was also simulated [15]. In this work, the soft contact model is further extended to control the position trajectory of the center of mass (CM) of a rigid disc using two soft material pads.

Object manipulation can be achieved by applying controlled forces and moments on the object at the contact interfaces. In this work, a cylindrical disc is taken as a rigid object. The object is grasped between two soft pads and rolled along the desired displacement trajectory. A closed-loop feedback controller is essential to measure the object's instantaneous position and generate the required force for control. An adaptive controller may be used for position and force control while handling a rigid object of unknown shape in an unknown environment [16]. In this work, a proportional-derivative (PD) controller is used to control the position trajectory of the disc's CM.

The outline of the paper is as follows. Bond graph models for dynamics of the rigid object and the two soft pads are developed. The object is grasped and rolled between the two soft pads, one above and the other below. Contact areas develop between the object and the soft pads during manipulation. Next, bond graph models are developed for contact interfaces. The model for rigid body dynamics is integrated with the models of the soft pads and the contact interfaces in Sec. 2. Section 3 discusses the bond graph model for the PD controller that generates the required forces to grasp and move the object along the desired displacement trajectory. The developed controller model is integrated with the model of the remaining system. The bond graph model is simulated and results are also presented. The conclusion and scope for future work are presented at the end.

2. BOND GRAPH MODELING

A system consisting of a rigid cylindrical disc resting on a soft material pad is considered. Bond graph models for a rigid body dynamics, soft material pad, and contact interface had been developed and integrated to model the overall system in [7]. The disc is placed on the soft pad. It deforms the pad due to its weight and contacts over an area. The developed model determines the contact area, the distribution of the contact forces over it and captures the pattern of deformed layers of the soft pad. The model is validated experimentally. The disc is then rolled over the soft pad such that its center of mass (CM) follows the desired displacement trajectory. The contact area and distribution of the contact forces change dynamically as the disc rolls over the soft pad. The model determines the continuously changing contact area and distribution of contact forces at the contact interface. A proportional and derivative (PD) controller is used to generate the required force to control the position of the disc's CM, and the force is applied at the disc's CM.

In this work, the soft contact model presented in [7] is further extended to control the position of the object's CM along the desired position trajectory by rolling it between two soft pads.

The system considered for rigid object manipulation consists of a rigid cylindrical disc and two soft material pads, as shown in Fig. 1. The system is considered in two dimensions. The disc is presented as the red circle, and its CM is at point C . The continuum of the soft material pads is discretized into a number of quadrilateral elements and nodes. Each pad is discretized into N number of nodes, each of two degrees of freedom. The soft material pads are shown by two meshed rectangles of length L_x and height L_y , one above and the other below the disc in Fig. 1. The upper pad is enclosed in a rigid bracket. C_{Br} is the bracket's CM. Initially, the disc is placed on the lower pad at its midpoint and grasped in the middle of the pads by applying a vertical downward force

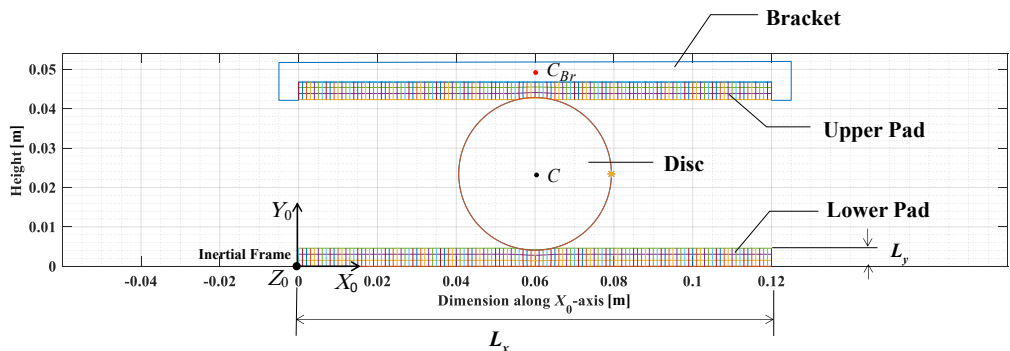


FIG. 1. The system considered for the soft contact manipulation of a rigid object.

on the CM of the bracket. The grasped disc in the middle of the pads is shown in Fig. 1. Then, the disc is rolled between the pads such that its CM moves horizontally along the desired displacement trajectory. The disc is rolled by applying horizontal controlled force on the bracket's CM. The controlled force is transmitted from the bracket to the contact interface through the soft pad and distributed over the contact area on the disc surface. The model determines the instantaneous required force distribution over the contact interface to achieve the desired manipulation compared to the required force applied at the disc's CM in [7].

Area contacts develop at the contact interfaces as the disc is grasped and rolled between the pads. A number of nodes contact the disc periphery at each instant during the object manipulation. A contact algorithm is developed to detect the instantaneous contacting nodes at the contact interfaces.

An inertial frame $\{\mathbf{O}\}$ with axes X_0 , Y_0 , and Z_0 is taken at the bottom-left corner of the lower pad. The notation ${}^A_B\bar{r}_C$ represents the position of point C with respect to point B expressed in the frame $\{\mathbf{A}\}$. ${}^0_C\bar{r}_C = \{x_C \ y_C \ z_C\}^T$ is the position vector of the disc's CM observed and expressed in the inertial frame, as shown in Fig. 2. The i -th node on the top layer of the lower pad is represented as node L_i and ${}^0_{\bar{r}_{L_i}}$ is its instantaneous position vector. The position of the node L_i with respect to the disc's CM of at any instant is given as:

$${}^0_C\bar{r}_{L_i} = {}^0_{\bar{r}_{L_i}} - {}^0_C\bar{r}_C. \quad (1)$$

Any node L_i contacts or penetrates the disc if $|{}^0_C\bar{r}_{L_i}| \leq$ (radius of the disc). In that case, the node L_i is re-designated as node S_i till it remains in contact with the disc. The initial contact point of the node S_i on the disc's periphery is represented as the point P_i .

Any j -th node on the bottom layer of the upper pad is labeled as node U_j . The position of the node U_j with respect to the center of mass C of the disc is ${}^0_C\bar{r}_{U_j}$. If the distance of the node U_j from the disc's CM is less than or equal to the disc's radius, it penetrates or contacts the disc. The contacting node is re-designated as node V_j , and it contacts the disc initially at the point Q_j , as shown in Fig. 2.

The velocity of the contact point P_i on the disc, observed and expressed in the inertial frame is given as:

$${}^0_{\dot{\bar{r}}_{P_i}} = {}^0_{\dot{\bar{r}}_C} + {}^0_C\dot{\bar{r}}_{P_i} = {}^0_{\dot{\bar{r}}_C} - [{}^0_C\bar{r}_{P_i} \times] {}^0_{\dot{\bar{\omega}}_D}, \quad (2)$$

where ${}^0_{\dot{\bar{r}}_C}$ is the velocity of the disc's CM and ${}^0_{\dot{\bar{\omega}}_D}$ is the disc's angular velocity, as observed and expressed in the inertial frame $\{\mathbf{O}\}$. $[{}^0_C\bar{r}_{P_i} \times]$ is a skew-symmetric matrix. The velocities ${}^0_{\dot{\bar{r}}_C}$ and ${}^0_C\dot{\bar{r}}_{P_i}$ are added at flow summing junction $0_0\bar{F}_{P_i}$ in the bond graph model, as shown in Fig. 3. $[{}^0_C\bar{r}_{P_i} \times]$ acts as modulus of the

with the rolling disc. ${}^0\bar{r}_{P_i}$ is the position of the point P_i with respect to the node S_i expressed in the inertial frame and given as:

$${}^0\bar{r}_{P_i} = [{}^0R] {}^i\bar{r}_{P_i}, \quad (3)$$

where ${}^i\bar{r}_{P_i} = \left\{ {}^i r_{P_{iT}} \quad {}^i r_{P_{iN}} \quad {}^i r_{P_{iZ}} \right\}$ is the position of the point P_i with respect to the node S_i expressed in the i -th moving frame. $[{}^0R] \in \mathbb{R}^{3 \times 3}$ is a rotational matrix that gives the orientation of the i -th moving frame with respect to the inertial frame. The determination of $[{}^0R]$ has been explained in detail in the reference [7]. The relative velocity of the point P_i with respect to the node S_i , observed and expressed in the inertial frame $\{O\}$ is given as:

$${}^0\dot{\bar{r}}_{P_i} = [{}^0\dot{R}] {}^i\bar{r}_{P_i} + [{}^0R] {}^i\dot{\bar{r}}_{P_i} = [{}^0\bar{\omega}_D \times] {}^0\bar{r}_{P_i} + [{}^0R] {}^i\dot{\bar{r}}_{P_i}. \quad (4)$$

The relative velocity ${}^i\dot{\bar{r}}_{P_i} = \left\{ {}^i \dot{r}_{P_{iT}} \quad {}^i \dot{r}_{P_{iN}} \quad {}^i \dot{r}_{P_{iZ}} \right\}$ of the point P_i with respect to the node S_i , observed and expressed in the i -th moving frame is given as:

$${}^i\dot{\bar{r}}_{P_i} = [{}^iR] \left\{ [{}^0\bar{r}_{P_i} \times] {}^0\bar{\omega}_D + {}^0\dot{\bar{r}}_{P_i} \right\} = [{}^iR] \left\{ [{}^0\bar{r}_{P_i} \times] {}^0\bar{\omega}_D + ({}^0\dot{\bar{r}}_{P_i} - {}^0\dot{\bar{r}}_{S_i}) \right\}. \quad (5)$$

The kinematics relation as given in Eq. (5) is represented in the bond graph model, as shown in Fig. 4. The velocities $[{}^0\bar{r}_{P_i} \times] {}^0\bar{\omega}_D$, ${}^0\dot{\bar{r}}_{P_i}$ and $-{}^0\dot{\bar{r}}_{S_i}$ are added at the flow summing junction at $0_0\bar{F}_{S_i}$.

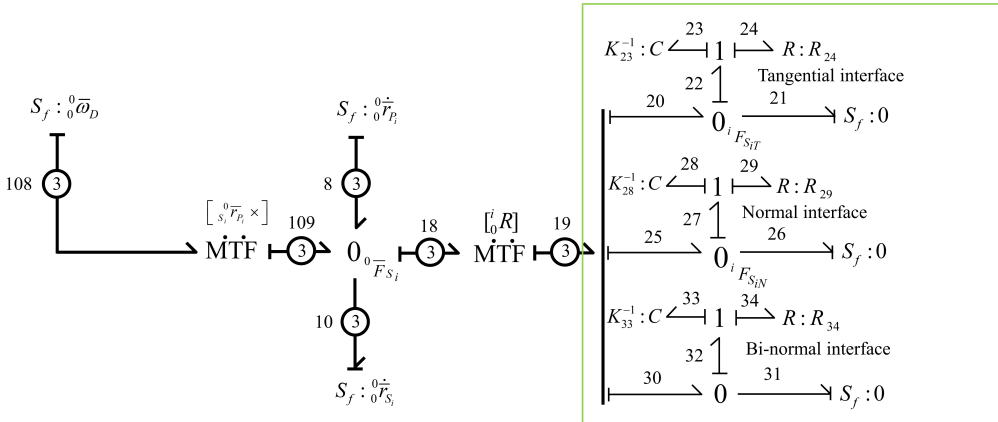


FIG. 4. The bond graph model for the lower contact interface.

From the law of conservation of energy, the resulting equation at $0_0\bar{F}_{S_i}$ junction is

$$\bar{f}_{18} = \bar{f}_{109} + \bar{f}_8 - \bar{f}_{10} = [{}^0\bar{r}_{P_i} \times] {}^0\bar{\omega}_D + {}^0\dot{\bar{r}}_{P_i} - {}^0\dot{\bar{r}}_{S_i}, \quad (6)$$

where the flow \bar{f}_{18} is the velocity of the point P_i with respect to the node S_i expressed in inertial frame $\{\mathbf{0}\}$. The velocity ${}_{S_i}^i \dot{\bar{r}}_{P_i}$ is determined using a modu-

lated transformer MTF, as shown in the bond graph model. The velocity ${}_{S_i}^i \dot{\bar{r}}_{P_i}$ is given as:

$${}_{S_i}^i \dot{\bar{r}}_{P_i} = \{ {}_{S_i}^i \dot{r}_{P_{iT}} \quad {}_{S_i}^i \dot{r}_{P_{iN}} \quad {}_{S_i}^i \dot{r}_{P_{iZ}} \} = \bar{f}_{19} = \{ f_{24} \quad f_{25} \quad f_{30} \}^T = [{}_{0}^i R] \bar{f}_{18}, \quad (7)$$

where the velocities ${}_{S_i}^i \dot{r}_{P_{iT}}$, ${}_{S_i}^i \dot{r}_{P_{iN}}$ and ${}_{S_i}^i \dot{r}_{P_{iZ}}$ are tangential, normal, and bi-normal component of the relative velocity ${}_{S_i}^i \dot{\bar{r}}_{P_i}$, respectively. The normal contact between the soft pad and the disc is modeled using the penalty approach. A spring and a dashpot in the Voigt model configuration are inserted between the node S_i and the contact point P_i , along the common normal direction at the lower interface, as shown in Fig. 2. The spring force prevents the penetration of the node S_i within the disc. The normal contact force ${}^i F_{P_{iN}}$ at the contact point P_i is calculated as:

$${}^i F_{P_{iN}} = -{}^i F_{S_{iN}} = -(K_{28} {}_{S_i}^i r_{P_{iN}} + R_{29} {}_{S_i}^i \dot{r}_{P_{iN}}) = -(e_{28} + e_{29}) = -e_{27}, \quad (8)$$

where K_{28} and R_{29} are the stiffness of the spring and damping coefficient of the dashpot inserted between the node S_i and the point P_i along the common normal at the lower contact interface, as shown in Fig. 2.

Similarly, for the upper contact interface, the j -th moving frame is considered at the point Q_j , with its axes along with the tangential and normal directions. The relative velocity ${}_{V_j}^j \dot{\bar{r}}_{Q_j}$ of the point Q_j with respect to the node V_j , observed and expressed in the j -th moving frame, is also calculated. The normal contact between the contact node V_j and the contact point Q_j is modeled similarly using the penalty approach. The normal contact force ${}^j F_{Q_{jN}}$ at the contact point Q_j is calculated as:

$${}^j F_{Q_{jN}} = -{}^j F_{V_{jN}} = -(K_{64} {}_{V_j}^j r_{Q_{jN}} + R_{65} {}_{V_j}^j \dot{r}_{Q_{jN}}) = -(e_{64} + e_{65}) = -e_{63}, \quad (9)$$

where K_{64} and R_{65} are stiffness of the spring and damping coefficient of the dashpot inserted between the node V_j and the point Q_j along the common normal at the upper contact interface. ${}_{V_j}^j \dot{\bar{r}}_{Q_{jN}}$ is the normal component of the relative velocity ${}_{V_j}^j \dot{\bar{r}}_{Q_j}$. The bond graph model for the upper contact interface is shown in Fig. 5.

The friction model based on Coulomb's law for dry friction is the simplest and the most used. However, the existence of discontinuity at zero relative velocity, as shown in Fig. 6, makes it numerically indeterminate.

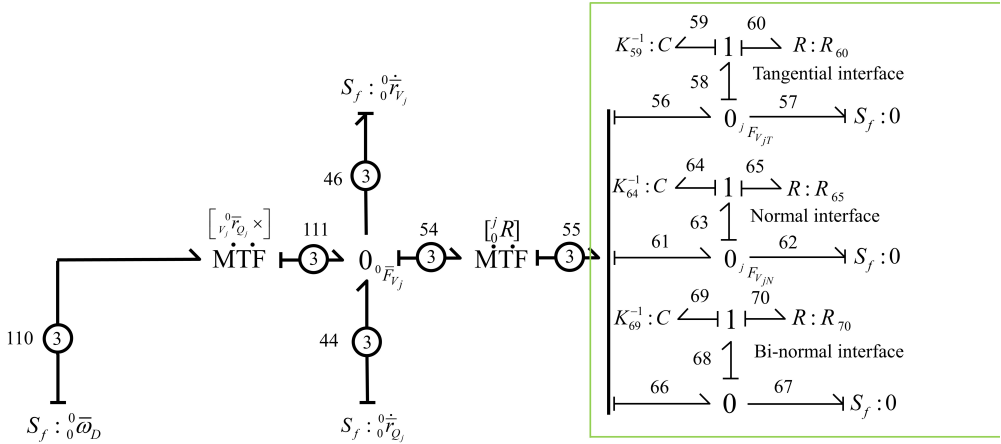


FIG. 5. The bond graph model for the upper contact interface.

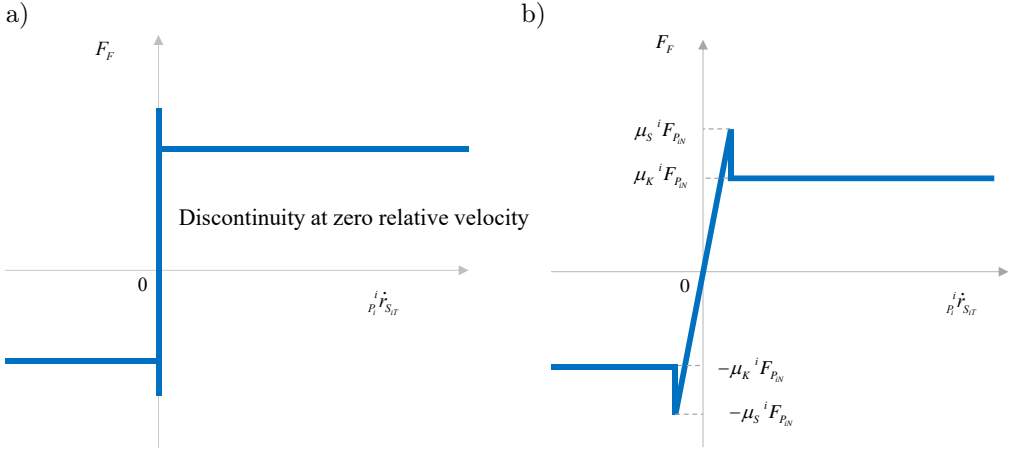


FIG. 6. a) Classical Coulomb's friction model, b) proposed friction model using momentary spring-dashpot in Kelvin-Voigt configuration.

The friction is modeled considering a momentary spring-dashpot in the Voigt model configuration along the common tangent at the point of contact as shown in Fig. 2. The tangential forces at the points of contact are calculated as:

$${}^i F_{P_i \text{TAN}} = -{}^i F_{S_i \text{TAN}} = -(K_{23} {}^i \dot{r}_{P_i T} + R_{24} {}^i \dot{r}_{P_i T}) = -(e_{23} + e_{24}) = -e_{20}, \quad (10)$$

$${}^j F_{Q_j \text{TAN}} = -{}^j F_{V_j \text{TAN}} = -(K_{59} {}^j \dot{r}_{Q_j T} + R_{60} {}^j \dot{r}_{Q_j T}) = -(e_{59} + e_{60}) = -e_{56}, \quad (11)$$

where ${}^i F_{P_i \text{TAN}}$ and ${}^j F_{Q_j \text{TAN}}$ are the tangential forces at contacting points P_i and Q_j , respectively, R_{24} and R_{60} are damping coefficients, ${}^i \dot{r}_{P_i T}$ and ${}^j \dot{r}_{Q_j T}$ are

components of the relative velocities in the tangential direction. Mathematically, the static and kinetic friction are modeled as:

$${}^i F_{P_i T} = \begin{cases} {}^i F_{P_i \text{TAN}}; & {}^i F_{P_i \text{TAN}} \leq \mu_S {}^i F_{P_i N}, \\ -\text{sgn}\left(\dot{S}_i \dot{r}_{P_i T}\right) \mu_K {}^i F_{P_i N}; & {}^i F_{P_i \text{TAN}} > \mu_S {}^i F_{P_i N}. \end{cases} \quad (12)$$

The friction force ${}^j F_{Q_j T}$ that acts on the contact point Q_j is determined as:

$${}^j F_{Q_j T} = \begin{cases} {}^j F_{Q_j \text{TAN}}; & {}^j F_{Q_j \text{TAN}} \leq \mu_S {}^j F_{Q_j N}, \\ -\text{sgn}\left(\dot{V}_j \dot{r}_{Q_j T}\right) \mu_K {}^j F_{Q_j N}; & {}^j F_{Q_j \text{TAN}} > \mu_S {}^j F_{Q_j N}. \end{cases} \quad (13)$$

The contact forces ${}^i \bar{F}_{P_i}$ and ${}^j \bar{F}_{Q_j}$ that act on the point P_i and Q_j expressed in i -th and j -th moving frame, respectively, are given as:

$${}^i \bar{F}_{P_i} = \left\{ {}^i F_{P_i T} \quad {}^i F_{P_i N} \quad 0 \right\}^T \quad \text{and} \quad {}^j \bar{F}_{Q_j} = \left\{ {}^j F_{Q_j T} \quad {}^j F_{Q_j N} \quad 0 \right\}^T. \quad (14)$$

The contact forces ${}^0 \bar{F}_{P_i}$ and ${}^0 \bar{F}_{Q_j}$ expressed in the inertial frame are given as:

$${}^0 \bar{F}_{P_i} = \begin{bmatrix} 0 \\ i \\ R \end{bmatrix} {}^i \bar{F}_{P_i} \quad \text{and} \quad {}^0 \bar{F}_{Q_j} = \begin{bmatrix} 0 \\ j \\ R \end{bmatrix} {}^j \bar{F}_{Q_j}. \quad (15)$$

The total force ${}^0 \bar{F}_D$ that acts on the disc is the vector sum of the forces acting on the disc's contact points at its contact interfaces and is given as:

$${}^0 \bar{F}_D = \sum_{i=1}^{T_L} {}^0 \bar{F}_{P_i} + \sum_{j=1}^{T_U} {}^0 \bar{F}_{Q_j}, \quad (16)$$

where T_L and T_U are the total numbers of contacting nodes of the lower and the upper pad, respectively, at any instant. The total force that results in the rate of change of the disc's translation momentum ${}^0 \bar{p}_D$ is given as:

$$\frac{d}{}^0 \bar{p}_D = {}^0 \bar{F}_D + {}^0 \bar{W}_D, \quad (17)$$

where ${}^0 \bar{W}_D = \{0 \quad -mg \quad 0\}^T$ is the disc's weight. The forces acting on the contact points of the disc produce moments about its CM. The rate of change of the angular momentum ${}^0 \bar{c} \bar{p}_D$ of the disc about its CM is given as:

$$\frac{d}{}^0 \bar{c} \bar{p}_D = \frac{d}{}^0 \bar{c} \bar{p}_D = \sum_{i=1}^{T_L} \left[{}^0 \bar{r}_{P_i} \times \right] {}^0 \bar{F}_{P_i} + \sum_{j=1}^{T_U} \left[{}^0 \bar{r}_{Q_j} \times \right] {}^0 \bar{F}_{Q_j}, \quad (18)$$

where ${}^0 [{}_C I_D]$ is the inertia tensor of the disc about its CM, expressed in the inertial frame. The forces that act on the contacting nodes S_i and V_j are equal and

opposite to the forces acting on the contacting points P_i and Q_j , respectively, and are given as:

$${}^0\bar{F}_{S_i} = -{}^0\bar{F}_{P_i} \quad \text{and} \quad {}^0\bar{F}_{V_j} = -{}^0\bar{F}_{Q_j}. \quad (19)$$

The contact forces ${}^0\bar{F}_{S_i}$ and ${}^0\bar{F}_{V_j}$ are represented as the source of efforts $S_e : {}^0\bar{F}_{S_i}$ at the lower interface and $S_e : {}^0\bar{F}_{V_j}$ at the upper interface, respectively, and are shown in the bond graph model in Fig. 7.

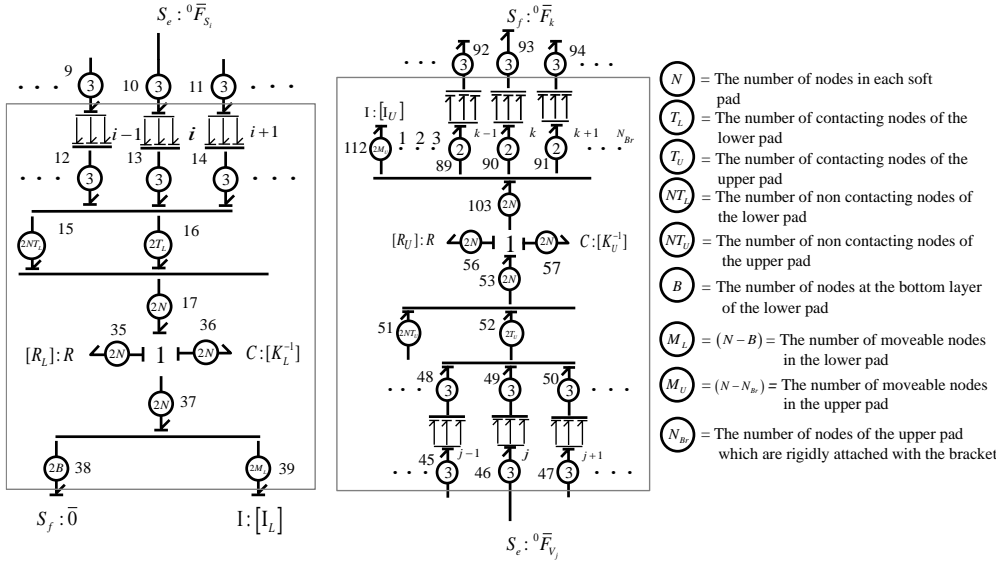


FIG. 7. The bond graph model for lower and upper soft material pads.

The continuum of the soft material is discretized. FEM is used to calculate the stiffness and inertia matrices of the soft material, which are used as \mathbf{C} and \mathbf{I} field, respectively, in the bond graph model. The damping of the soft material is modeled as a constant \mathbf{R} field. The methodology for discretization and computation of the stiffness, damping, and inertia matrices has been presented in detail in [11]. $[K_L] \in \mathbb{R}^{2N \times 2N}$, $[R_L] \in \mathbb{R}^{2N \times 2N}$ are stiffness and damping matrices for the lower pad, and modeled as \mathbf{C} -field $C : [K_L]^{-1}$; $[K_U] \in \mathbb{R}^{2N \times 2N}$ and \mathbf{R} -field $R : [R_U]$; $[R_U] \in \mathbb{R}^{2N \times 2N}$, respectively, in the bond graph model, as shown in Fig. 7. The bottom layer of the lower pad is fixed to the ground and constrained using $S_f : \bar{0} \in \mathbb{R}^{2B}$. The number of nodes on the bottom layer is B . Consequently, inertia is not attributed to these stationary nodes. The inertia matrix $[I_L] \in \mathbb{R}^{2(N-B) \times 2(N-B)}$ is calculated considering the masses of the remaining $(N - B)$ movable nodes and modeled as \mathbf{I} -field $I : [I_L]$; $[I_U] \in \mathbb{R}^{2(N-B) \times 2(N-B)}$ in the bond graph model, as shown in Fig. 7. Both the soft pads are silicon rubber pads. The stiffness and damping matrices for the upper pad are calculated

similarly and represented as **C**-field $C : [K_U]^{-1}$; $[K_U] \in \mathbb{R}^{2N \times 2N}$ and **R**-field $R : [R_U]$; $[R_U] \in \mathbb{R}^{2N \times 2N}$, respectively. The upper pad is enclosed in a rigid bracket, as shown in Fig. 1. The total N_{Br} nodes in contact with the bracket are rigidly attached to it. Hence, the masses of these nodes are not included in the inertia matrix of the upper pad. The inertia matrix is calculated considering the masses of the remaining $(N - N_{Br})$ nodes and represented as **I**-field $I : [I_U]$; $[I_U] \in \mathbb{R}^{2(N - N_{Br}) \times 2(N - N_{Br})}$ in the bond graph model, as shown in Fig. 7. Source of flow $S_f : {}^0\dot{\bar{v}}_{Br}$ represents the velocity of the bracket, and the nodes rigidly attached to the bracket move with the same velocity as the bracket moves. The bond graph model for the bracket is shown in Fig. 8. The source $S_e : {}^0\bar{F}_k$ represents the effort received by the bracket at one of the rigidly connected k -th nodes among N_{Br} nodes.

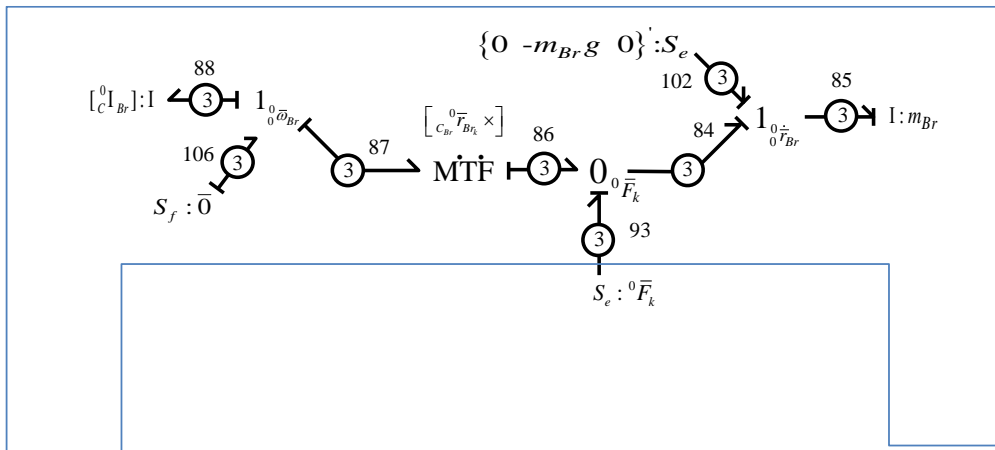


FIG. 8. The bond graph model for the rigid bracket connected rigidly with nodes on the upper layer of the upper soft pads.

The rotation of the bracket about its CM is constrained using $S_f : \bar{0}$, but it is allowed to translate horizontally. The bond graph models of the rigid body dynamics, the soft pads, the contact interfaces are integrated and connected with intermediate bonds, as shown in Fig. 9. The bond graph model represents the dynamics of the disc and the soft pads along with the dynamics at the contact interfaces.

The desired displacement trajectory for the disc’s CM is defined. The disc is grasped and rolled between the pads such that its CM follows the desired trajectory. A closed-loop feedback controller is used to determine the disc’s instantaneous position and generate the required forces for grasping and rolling the disc along the desired displacement trajectory. The bond graph modeling of the closed-loop feedback control system and simulation results are presented in the next section.

The radius of the disc is taken as 19.37 mm. The center of mass of the disc is at $x_c(0) = 60$ mm and $y_c(0) = 23.20$ mm. The dimensions of both the pads are taken to be equal. The length and height of the pads are $L_x = 120$ mm and $L_y = 4.59$ mm, respectively. The bottom surface of the lower pad is fixed to the ground. The upper pad is enclosed in the rigid bracket of mass m_{Br} . $C_{Br}(x_{Br}, y_{Br})$ is the CM of the bracket, as shown in Fig. 1. The bracket is pressed downward to grasp the disc in the middle of the two pads and kept at the same vertical position during its horizontal motion.

The disc is rolled horizontally by applying a controlled force on the bracket's CM along the X_0 -axis of the inertial frame. The bracket's rotational motion is constrained. Hence, it can only translate.

The displacement trajectory of the disc's CM is defined such that it moves 20 mm in 10 s along the negative X_0 -axis and stays there for 5 s. It is rolled back to the initial position in the next 10 s. The velocity, acceleration, and jerk at the starting and the end of the motion of the disc are kept zero. The displacement trajectory is defined by a polynomial as given in Eq. (20), and Eq. (21) is a polynomial for the corresponding desired velocity profile,

$$x_d(t) = c_0 + c_1t + c_2t^2 + c_3t^3 + c_4t^4 + c_5t^5 + c_6t^6 + c_7t^7, \quad (20)$$

$$\dot{x}_d(t) = c_1 + 2c_2t + 3c_3t^2 + 4c_4t^3 + 5c_5t^4 + 6c_6t^5 + 7c_7t^6, \quad (21)$$

where $x_d(t)$, $\dot{x}_d(t)$ are the desired displacement and velocity of the disc's CM at any time t and c_0, c_1, \dots, c_7 are constant coefficients. The instantaneous position of the disc's CM is ${}^0\vec{r}_C(t) = \{x_C(t) \ y_C(t) \ z_C(t)\}^T$. The disc's CM is moved towards the left by 20 mm. The initial and final conditions for desired and actual displacements of the disc's CM during the period from 0 to 10 s are:

$$x_d(0) = x_C(0) = 60 \text{ mm}, \quad (22)$$

$$x_d(10) = x_C(0) - 20 \text{ mm}, \quad (23)$$

$$\dot{x}(0) = 0; \quad \ddot{x}_d(0) = 0; \quad \dddot{x}_d(0) = 0 \quad \text{and} \quad (24)$$

$$\dot{x}_d(10) = 0; \quad \ddot{x}_d(10) = 0; \quad \dddot{x}_d(10) = 0,$$

the values of the coefficients c_0, c_1, \dots, c_7 are determined for the trajectory during this time interval based on the above conditions, where $\ddot{x}_d(t)$, $\dddot{x}_d(t)$ are the acceleration and jerk, respectively, at any time t . The disc stays at this position for the next 5 s, hence:

$$x_d(t) = x_C(10), \quad 10 \leq t \leq 15, \quad (25)$$

$$\dot{x}_d(t) = 0, \quad 10 \leq t \leq 15. \quad (26)$$

The disc is then rolled back to its initial position in the next 10 s. The initial and final conditions for this displacement trajectory are:

$$x_d(15) = x_C(10), \quad (27)$$

$$x_d(25) = x_C(0), \quad (28)$$

$$\dot{x}_d(15) = 0; \quad \ddot{x}_d(15) = 0; \quad \dddot{x}_d(15) = 0 \quad \text{and} \quad (29)$$

$$\dot{x}_d(25) = 0; \quad \ddot{x}_d(25) = 0; \quad \dddot{x}_d(25) = 0.$$

The values of the coefficients c_0, c_1, \dots, c_7 are determined for the trajectory during this time interval based on the conditions given in (27)–(29). The desired displacement trajectory and the velocity profile with respect to time are shown in Fig. 10a and Fig. 10b, respectively.

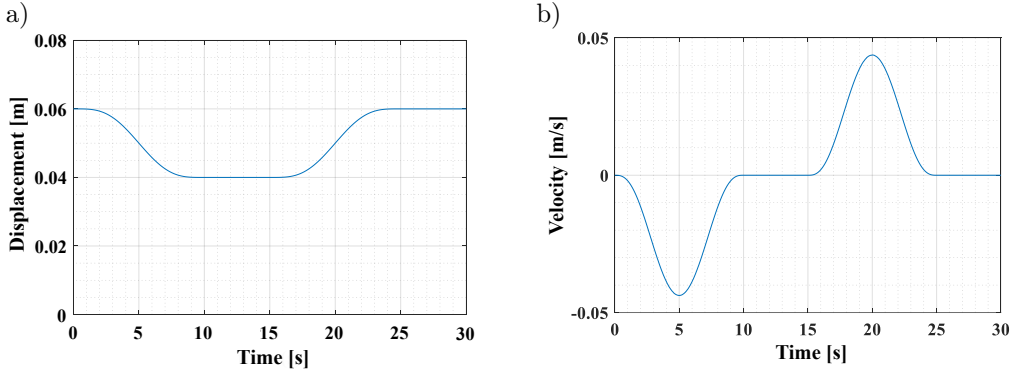


FIG. 10. a) Desired displacement trajectory, b) desired velocity profile.

The disc is grasped between the two pads by applying a vertical downward force at the brackets CM. In the grasped posture, the total deformation in both the soft pads is 1.5 mm, and the bracket's CM C_{Br} is at $x_{Br}(t_g) = 60$ mm and $y_{Br}(t_g) = 48.6$ mm, where t_g is the time taken to grasp the disc. The vertical movement of the bracket is constrained hereafter, i.e., during its controlled horizontal motion. A proportional – derivative (PD) controller is used to restrict the vertical motion of the bracket. The desired instantaneous vertical position $y_{Brd}(t)$ and velocity $\dot{y}_{Brd}(t)$ of the bracket's CM are:

$$y_{Brd}(t) = y_{Br}(t_g) = 48.6 \text{ mm} \quad \text{and} \quad \dot{y}_{Brd}(t) = \dot{y}_{Br}(t_g) = 0 \text{ mm/s}. \quad (30)$$

An activated bond in the bond graph model only carries the information of effort or flow but not power. The activated bond in Fig. 9, attached to the $1_0 \dot{\vec{r}}_{Br}$ junction, carries the information of flow, which is the instantaneous actual

velocity of the bracket's CM. It acts as a velocity feedback sensor for the PD controller. The instantaneous position $E_v(t)$ and velocity $\dot{E}_v(t)$ errors due to vertical displacement of the bracket are given as:

$$E_v(t) = y_{Brd}(t) - y_{Br}(t) \quad \text{and} \quad \dot{E}_v(t) = \dot{y}_{Brd}(t) - \dot{y}_{Br}(t), \quad (31)$$

where $y_{Br}(t)$ and $\dot{y}_{Br}(t)$ are the instantaneous vertical position and velocity of the CM of the bracket, respectively.

In case of any vertical movement of the bracket from its desired vertical position, the PD controller generates a vertical force applied at the bracket's CM. Hence, it prevents the bracket's vertical displacement during its horizontal motion. The generated vertical force ${}^0F_y(t)$ is given as:

$${}^0F_y(t) = K_{98}E_v(t) + R_{99}\dot{E}_v(t), \quad (32)$$

where $K_{98} = 1.2 \times 10^5$ N/m and $R_{99} = 441.7149$ N·s/m are the proportional and derivative gains of the PD controller, which correspond to the stiffness and damping coefficients in the subsystem elements $C : K_{98}^{-1}$ and $R : R_{99}$. Figure 11a shows ${}^0F_y(t)$ with respect to time t . Initially, the disc is grasped at time $t_g = 0.375$ s, and the vertical downward grasping force is applied at time t_g , as shown in Fig. 11a. The bracket's vertical movement is constrained during its horizontal motion. Hence, the force ${}^0F_y(t)$ does not vary much during the rolling of the disc.

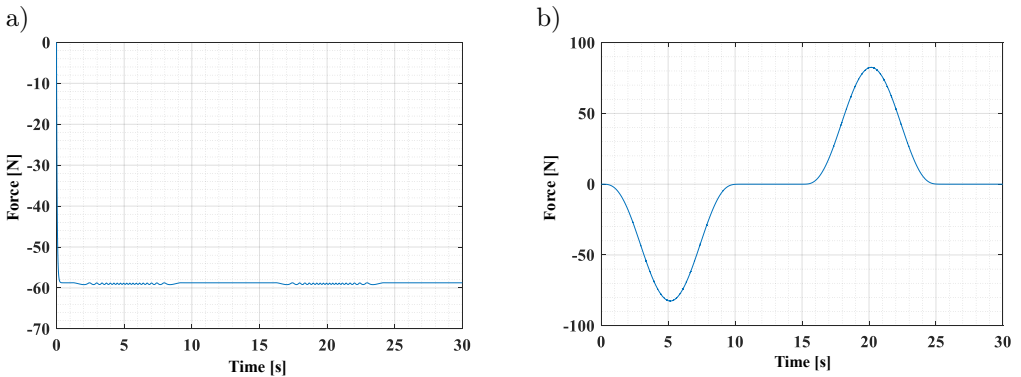


FIG. 11. a) Vertical force ${}^0F_y(t)$ versus time, b) horizontal force ${}^0F_x(t)$ versus time.

The second PD controller is used to control the horizontal position of the disc's CM. It measures the actual velocity $\dot{x}_C(t)$ and compares it with the disc's desired instantaneous velocity $\dot{x}_d(t)$. The instantaneous position error $E_h(t)$ and velocity error $\dot{E}_h(t)$ are given as:

$$E_h(t) = x_d(t) - x_C(t) \quad \text{and} \quad \dot{E}_h(t) = \dot{x}_d(t) - \dot{x}_C(t), \quad (33)$$

where $x_C(t)$ is the instantaneous abscissa of the disc's CM. In the case of non-zero position error, the PD controller generates the horizontal force which is given as:

$${}^0F_x(t) = K_{81}E_h(t) + R_{80}\dot{E}_h(t), \quad (34)$$

where $K_{81} = 1.2 \times 10^5$ N/m and $R_{80} = 441.7149$ N·s/m are the proportional and derivative gains of the PD controller, which correspond to the stiffness and damping coefficients in the subsystem elements $C : K_{81}^{-1}$ and $R : R_{80}$. The force component ${}^0F_x(t)$ with respect to time is shown in Fig. 11b.

The force ${}^0F_x(t)$ is applied at the bracket's CM to move it horizontally. The negative force in Fig. 11b implies that force is applied towards the left at the bracket's CM, and positive force implies the force applied in the right direction.

The contact forces at the upper soft contact interface produce moments on the bracket about its CM. The moment $\overline{M}_{C_{Br}}(t)$ that acts on the bracket about its CM at any instant is given as:

$$\overline{M}_{C_{Br}} = \bar{e}_{106} = - [{}_{C_{Br}}^0\bar{r}_{Br_k} \times] \bar{e}_{86}, \quad (35)$$

where ${}_{C_{Br}}^0\bar{r}_{Br_k}$ is the position of the k -th node rigidly attached to the bracket with respect to the bracket's CM expressed in the inertial frame. The moment $\overline{M}_{C_{Br}}(t)$ with respect to the time is shown in Fig. 12.

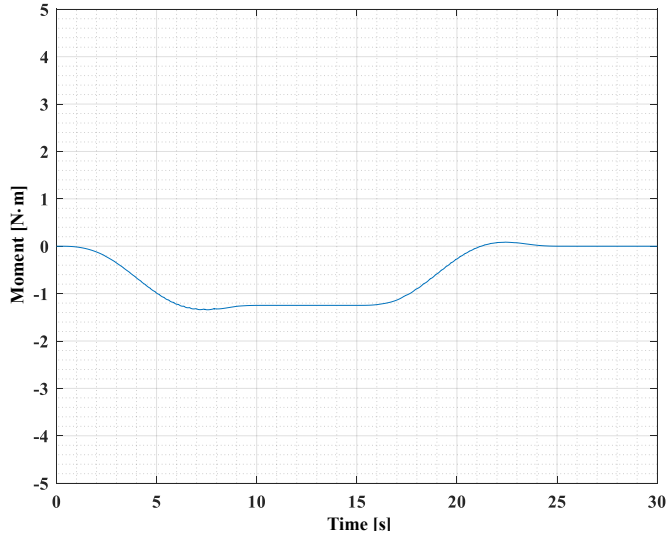


FIG. 12. The moment that acts on the bracket about its CM with respect to time.

The bracket is only allowed to translate horizontally and its rotation is constrained using the source of flow $S_f : \bar{0}$ connected to junction $1_{0\bar{\omega}_{Br}}$, as shown in the bond graph model in Fig. 8.

The actual position of the disc's CM with respect to time t is shown in Fig. 13a. Initially, the disc is at the midpoint $x_C(0) = 60$ mm of the pads. It rolls anticlockwise and reaches $x_C(10) = 40$ mm in 10 s. It stops here for the next 5 s and rolls back to its initial position at $x_C(25) = 60$ mm in the next 10 s. The curve in Fig. 13a shows the actual displacement trajectory of the disc's CM. It follows the desired displacement trajectory, as shown in Fig. 10a. The actual velocity ${}^0\dot{r}_C$ of the disc with respect to time is shown in Fig. 13b. Transients are noticeable at several points on this velocity profile. These transients are due to the contact transitions from one discrete node to the other on the soft material pads as the disc rolls over it.

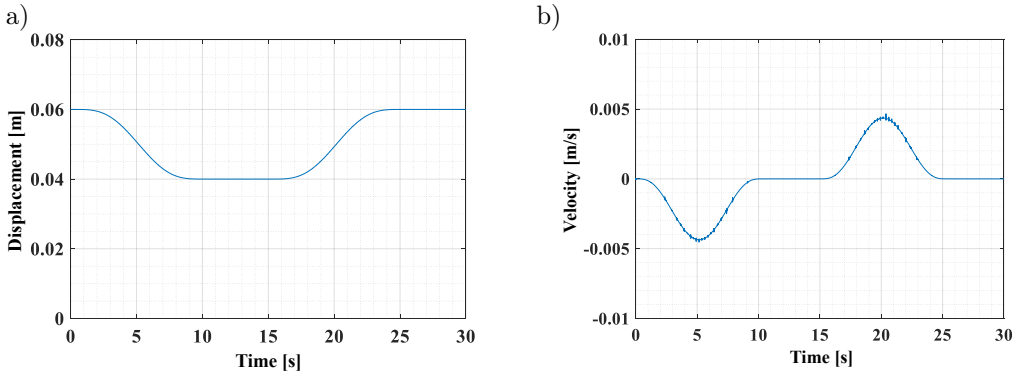


FIG. 13. a) Actual displacement trajectory of the disc's CM, b) actual velocity profile of the disc's CM.

The model determines the required contact forces to be applied on the disc at its contact interfaces for its position control. The contact forces at the contacting points are determined according to Eq. (14), as explained in Sec. 2. Initially, the disc is grasped between the two pads. The time taken to grasp the disc is $t_g = 0.375$ s. A snapshot that is taken at time $t = 0.125$ s during the grasping of the disc is shown in Fig. 14. The distribution of normal forces ${}^iF_{S_iN}$ and ${}^jF_{V_jN}$ at the lower and the upper contact interfaces is shown with the red curves in Figs. 14a and 14c, respectively. Normal forces compress the soft pads at the contact interfaces. Red-filled circles on the normal force curves represent the values of the normal contact forces on the respective nodes. The normal force is maximum at the center of the interface and decreases away from it on both sides.

The viscoelastic frictional forces ${}^iF_{P_iT}$ and ${}^jF_{Q_jT}$ act at contact points, where, ${}^iF_{S_iT}$ and ${}^jF_{V_jT}$ are the frictional forces acting at the contact nodes S_i and V_j , respectively, on the soft pads. These are equal and opposite to the frictional forces at the corresponding contact points P_i and Q_j , respectively, on the disc. The frictional force at the contact points is determined according to Eqs. (12) and (13), as explained in Sec. 2. The distribution of the friction at the upper and

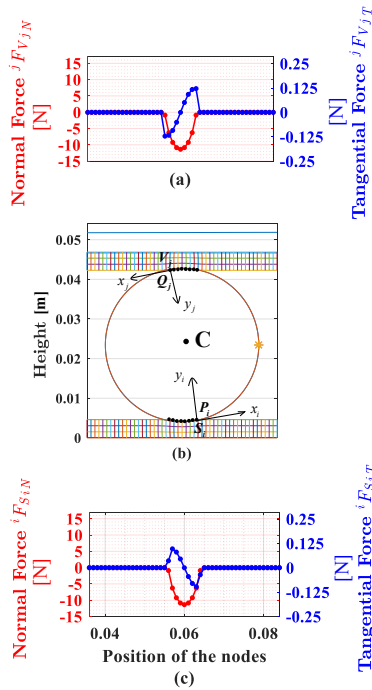


FIG. 14. Normal and frictional force distribution at $t = 0.125$ s during the grasping of the disc.

the lower contact interfaces is shown by the blue curves in Figs. 14a and 14c, respectively.

The node at the center of the contact interface does not move tangentially relative to the disc periphery during grasping. Hence, the frictional force is zero at the center of the contact interface. Contact nodes on both sides of the central node slide on the disc periphery during the grasping. The sliding of nodes over the disc periphery depends upon their positions with respect to the central node. The farther the node is from the center of the interface, the more it slides in a given time during grasping. Nodes at the extreme ends of the contact interfaces slide more as compared to the inner nodes nearer to the central node. Hence, friction at the extreme nodes of the contact interface is maximum. The friction is distributed equally and with opposite directions on both sides of the center of the contact interface. Hence, no resultant moment due to the frictional forces acts on the disc during grasping. In the grasped posture at time $t = 0.375$ s, as shown in Fig. 16a, friction does not act at the contact interfaces.

Then, the disc is rolled by applying a controlled horizontal force on the bracket's CM. A snapshot, shown in Fig. 15, is captured during the anticlockwise rolling of the disc at the time $t = 5$ s. The distribution of friction at the upper and the lower contact interfaces during the rolling of the grasped disc is

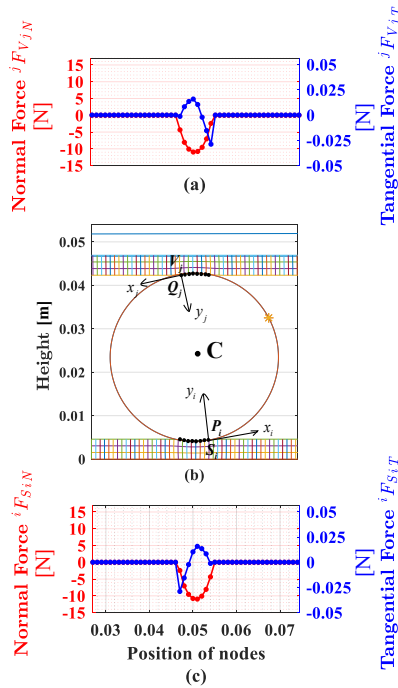
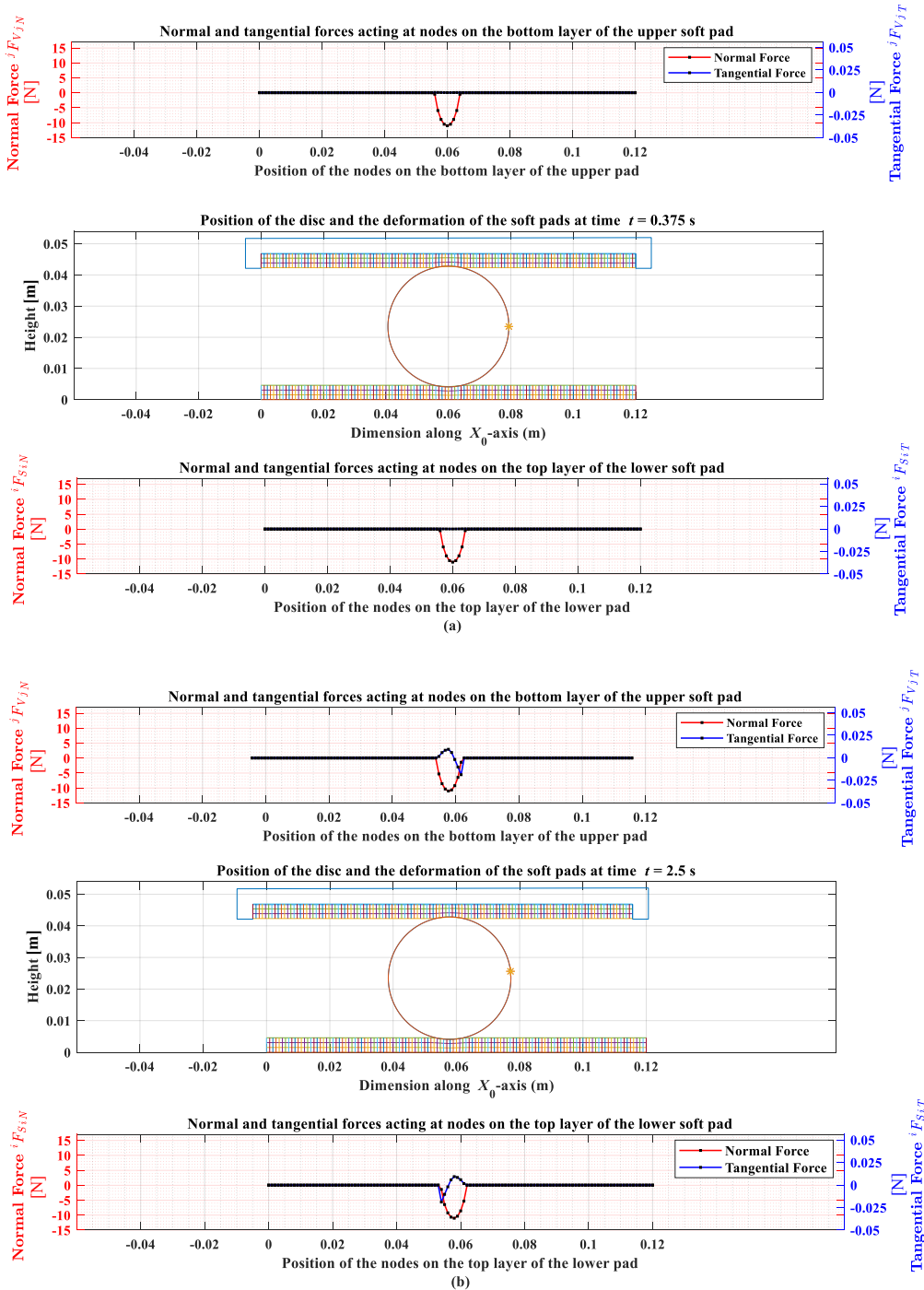


FIG. 15. Normal and frictional force distribution at $t = 5$ s during the anticlockwise rolling of the grasped disc.

shown by the blue curve in Figs. 15a and 15c, respectively. The friction is not distributed uniformly at the contact interface. The resultant moment due to the friction acts on the disc about its CM and produces a change in its angular momentum causing the rolling motion.

The position of the disc and the deformed layers of the soft pads, along with the distribution of contact forces over the contact interfaces at different instances, are shown by a series of snapshots in Figs. 16a–16i. The video attached as a file “Soft Contact Manipulation of a Rigid Object.avi” shows the simulation of the manipulation of the disc using the two soft pads.

Initially, the disc is grasped. Figure 16a shows the disc position, deformation in the layers of the pads after grasping, and just before the rolling of the disc at time $t = 0.375$ s. The distribution of contact forces shows that only the normal forces act at the contact points without friction at this instant. Then, it is rolled anticlockwise and its CM is moved by -20 mm along the X_0 -axis in the first 10 s. The disc position, deformed layers of the soft pads, and the distribution of contact forces at time instants $t = 2.5$ s, $t = 5$ s, $t = 7.5$ s, and $t = 10$ s are shown in Figs. 16b–16e, respectively. The disc then stops and remains at this position for the next 5 s.



[FIG. 16ab]

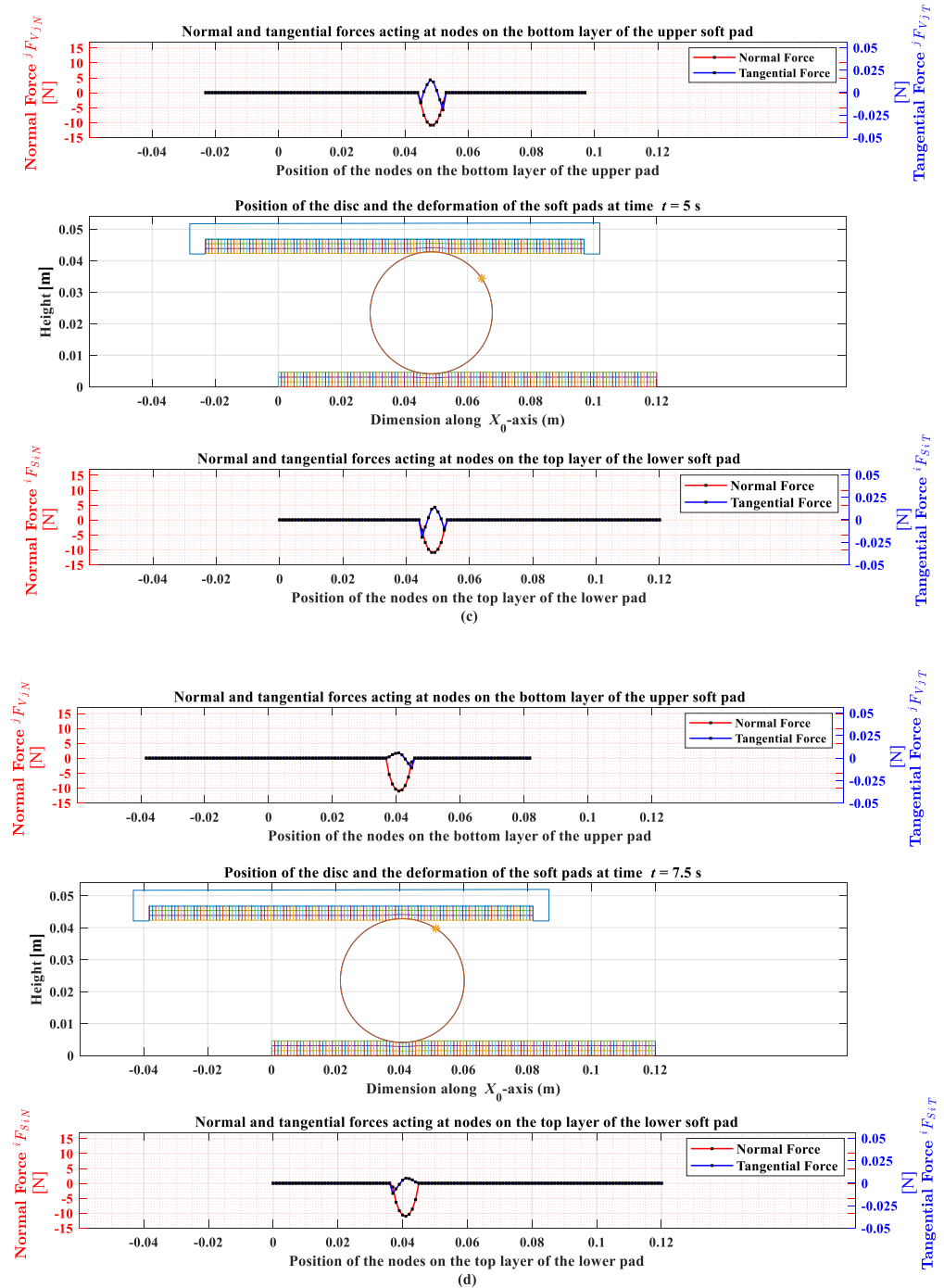


[FIG. 16cd]

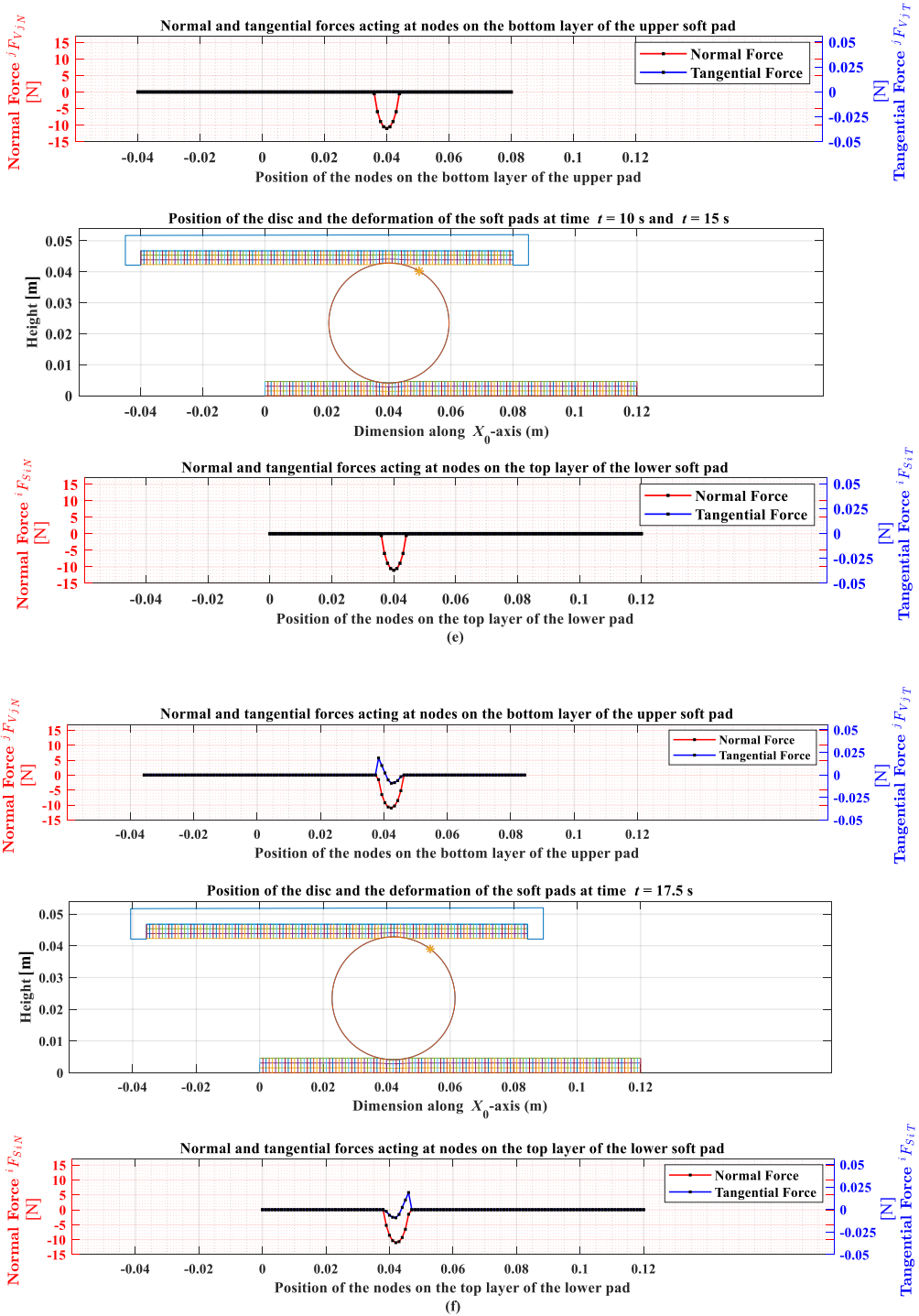


[FIG. 16ef]

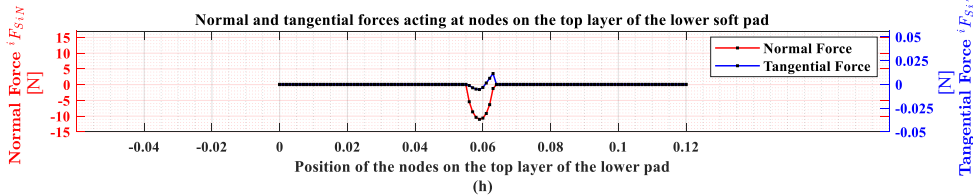
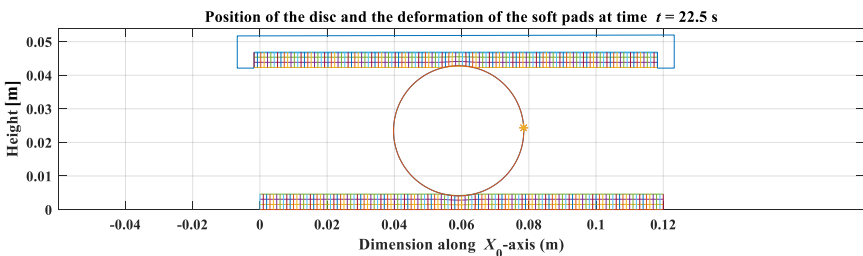
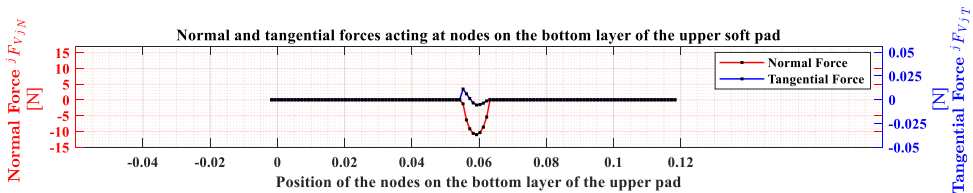
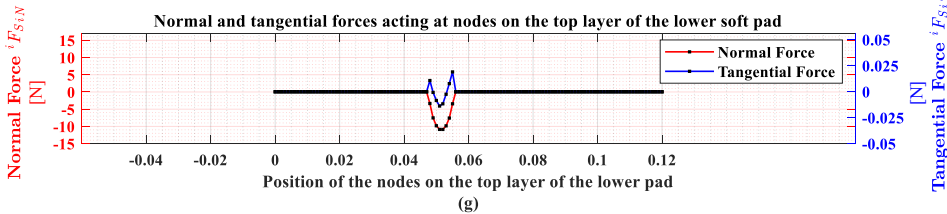
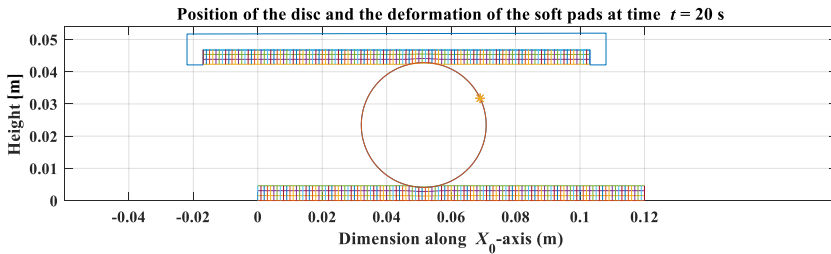
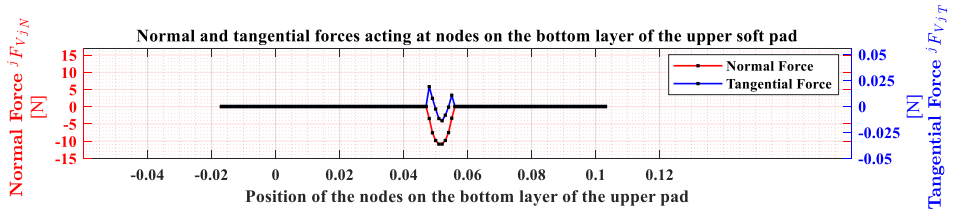


[FIG. 16gh]

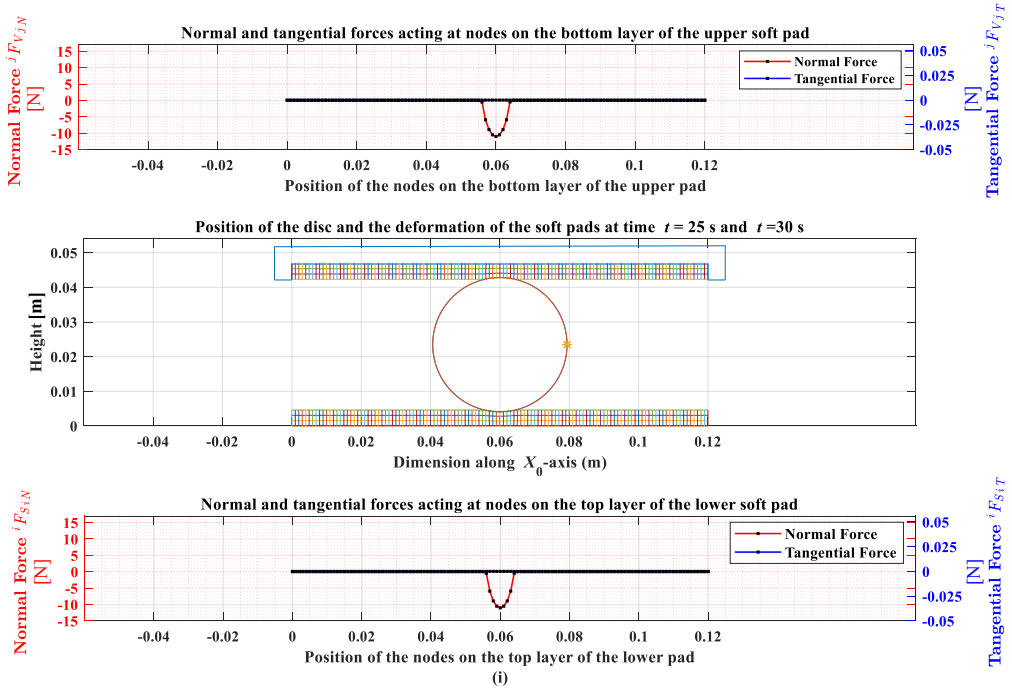


FIG. 16. The positions of the disc and the distribution of contact forces along with the deformation in layers of the soft pads at various instants of time: a) $t = 0.375$ s, b) $t = 2.5$ s, c) $t = 5$ s, d) $t = 7.5$ s, e) $t = 10$ s and $t = 15$ s, f) $t = 17.5$ s, g) $t = 20$ s, h) $t = 22.5$ s, i) $t = 25$ s and $t = 30$ s.

It starts rolling clockwise at the time $t = 15$ s from the position $x_C(10$ s) = 40 mm, shown in Fig. 16e. Its CM returns to its initial position in the next 10 s. The snapshots shown in Figs. 16e–16i are captured at time $t = 17.5$ s, $t = 20$ s, $t = 22.5$ s, and $t = 25$ s, respectively, while the disc rolls back to its initial position. Finally, it rests in a state of static equilibrium from $t = 25$ s to $t = 30$ s, as shown in Fig. 16i.

The angular momentum ${}^0\bar{p}_D$ of the disc about its CM, expressed in the inertial frame with respect to time t is shown in Fig. 17. The disc rotates anticlockwise as its CM translates towards the left and rotates clockwise about the Z_0 -axis while returning to its initial position. The angular momenta about X_0 -axis and Y_0 -axis are zero, as there is no rotational motion about these axes. The disc follows the desired displacement trajectory, and the model determines the instantaneous contact forces required to manipulate the disc along the desired displacement trajectory. The model is independent of the material of the soft pads, the geometry of the rigid object, and the trajectory chosen.

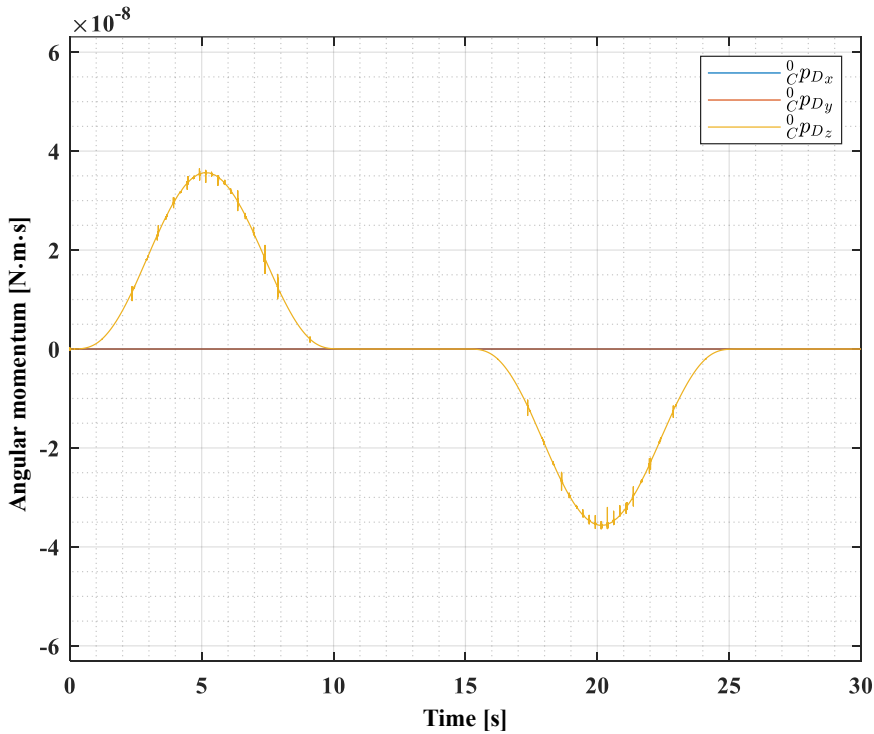


FIG. 17. The angular momentum of the disc with respect to time.

4. CONCLUSION

A multibond graph model has been developed to evaluate the dynamics of soft contact manipulation of a rigid object rolling between two soft pads. The model captures the dynamic pattern of the deformed layers of the soft pads. The model implements a PD controller for the position control of the CM of the rigid object. The control effort is applied to the bracket that holds the upper soft pad. The controller gains have physical significance and can be interpreted as stiffness and damping parameters in the bond graph model. The model determines the instantaneous contact areas and distribution of contact forces at the contact interfaces, which change dynamically during object manipulation. It also determines the instantaneous force distributions that must be applied at the contact interfaces for the desired manipulation of the object. The model is independent of the material of the soft pads, the geometry of the rigid object and is applicable for any desired input trajectory. The model may be extended further for the orientation control of rigid objects rolled between soft pads. This

work may further be extended to analyze object manipulation using a human hand with soft pulped fingertips.

REFERENCES

1. A. Bicchi, Hands for dexterous manipulation and robust grasping: A difficult road toward simplicity, *IEEE Transactions on Robotics and Automation*, **16**(6): 652–662, 2000.
2. A.M. Okamura, N. Smaby, M.R. Cutkosky, An overview of dexterous manipulation, [in:] *Proceedings 2000 ICRA, Millennium Conference, IEEE International Conference on Robotics and Automation*, vol. 1, pp. 255–262, 2000, doi: 10.1109/ROBOT.2000.844067.
3. P. Flores, M. Machado, M.T. Silva, J.M. Martins, On the continuous contact force models for soft material in multibody dynamics, *Multibody System Dynamics*, **25**(3): 357–375, 2011, doi: 10.1007/s11044-010-9237-4.
4. Z. Doulgeri, J. Fasoulas, S. Arimoto, Feedback control for object manipulation by a pair of soft tip fingers, *Robotica*, **20**(1): 1–11, 2002, doi: 10.1017/S0263574701003733.
5. K.L. Johnson, *Contact Mechanics*, Cambridge University Press, 1985.
6. K.L. Johnson, K. Kendall, A.D. Roberts, Surface energy and the contact of elastic solids, *Proceedings of the Royal Society London A*, **324**(1558): 301–313, 1971, doi: 10.1098/rspa.1971.0141.
7. A.K. Narwal, A. Vaz, K.D. Gupta, Study of dynamics of soft contact rolling using multi-bond graph approach, *Mechanism and Machine Theory*, **75**: 79–96, 2014, doi: 10.1016/j.mechmachtheory.2014.01.004.
8. A. Mukherjee, R. Karmakar, A.K. Samantaray, *Bond Graph in Modeling, Simulation and Fault Identification*, I.K. International, 2006.
9. D.C. Karnopp, D.L. Margolis, R.C. Rosenberg, *System Dynamics: Modeling and Simulation of Mechatronic Systems*, Wiley-Interscience, 2000.
10. J. Thoma, B. Ould Bouamama, *Modelling and Simulation in Thermal and Chemical Engineering, A Bond Graph Approach*, Springer-Verlag, Berlin, Heidelberg, New York, 2000.
11. W. Borutzky, *Bond Graph Methodology: Development and Analysis of Multidisciplinary Dynamic System Models*, Springer-Verlag, London, Dordrecht, Heidelberg, New York, 2010.
12. A.K. Narwal, A. Vaz, K.D. Gupta, Bond graph modeling of dynamics of soft contact interaction of a non-circular rigid body rolling on a soft material, *Mechanism and Machine Theory*, **86**: 265–280, 2015, doi: 10.1016/j.mechmachtheory.2014.12.010.
13. A.K. Narwal, A. Vaz, K.D. Gupta, Understanding soft contact interaction between a non-circular rigid body and a soft material using multi-bond graph, [in:] *Proceedings of the International Conference on Bond Graph Modeling and Simulation*, vol. 46, pp. 690–697, 2014.
14. A. Vaz, A. K. Narwal, K.D. Gupta, Evaluation of dynamics of soft contact rolling using multi-bond graph approach, [in:] *Proceedings of the 1st International and 16th National*

Conference on Machines and Mechanisms, IIT Roorkee, India, Dec. 18–20, pp. 23–29, 2013.

15. M. Sachdeva, A.K. Narwal, A. Vaz, Simulation of impact and rolling contact dynamics between a rigid body and a soft material using multibond graph approach, [in:] *Proceedings of the 2nd International and 17th National Conference on Machines and Mechanisms*, Dec. 16–19, 2015.
16. Z. Doulgeri, Y. Karayiannidis, Force position control for a robot finger with a soft tip and kinematic uncertainties, *Robotics and Autonomous Systems*, **55**(4): 328–336, 2007, doi: 10.1016/j.robot.2006.11.003.

Received September 5, 2021; revised version January 4, 2022.